Journal of Materials Chemistry A

Few-Layer Graphene-Graphene Oxide Composite containing Nanodiamonds as Metal-Free Catalyst

Journal:	*Journal of Materials Chemistry A*
Manuscript ID:	TA-ART-03-2014-001307.R1
Article Type:	Paper
Date Submitted by the Author:	22-Apr-2014

Complete List of Authors:	Pham-Huu, Cuong; CNRS, University of Strasbourg, ICPEES, UMR 7515 Tung, Tran Thanh; CNRS, University of Strasbourg, Ba, Houssienou; ICPEES, UMR 7515 CNRS- Université de Strasbourg (UdS), Lai, Truong Phuoc; ICPEES, UMR 7515 CNRS- Université de Strasbourg (UdS), Nhut, Jean-Mario; CNRS, University of Strasbourg, Ersen, Ovidiu; ICPMS, University of Strasbourg, Department of Surfaces and Interfaces Begin, Dominique; CNRS, University of Strasbourg, Janowska, Izabela; CNRS, University of Strasbourg, Nguyen, Dinh Lam; The University of Da-Nang, University of Science and Tecnology, Granger, Pascal; Unité de Catalyse et de Chimie du Solide, Université de Lille1, Sciences et Technologies,

Journal of Materials Chemistry A

Cite this: DOI: 10.1039/c0xx00000x

ARTICLE TYPE

www.rsc.org/xxxxxx

Few-Layer Graphene-Graphene Oxide Composite containing Nanodiamonds as Metal-Free Catalyst

Tung Tran Thanh[a], Housseinou Ba[a], Lai Truong-Phuoc[a], Jean-Mario Nhut[a], Ovidiu Ersen[b], Dominique Begin[a], Izabela Janowska[a], Dinh Lam Nguyen[c], Pascal Granger[d], Cuong Pham-Huu[a]*

[a]*Institut de Chimie et Procédés pour l'Energie, l'Environnement et la Santé (ICPEES), ECPM, UMR 7515 du CNRS-Université de Strasbourg, 25 rue Becquerel, 67087 Strasbourg Cedex 02, France.*
[b]*Institut de Physique et de Chimie des Matériaux de Strasbourg (IPCMS), UMR 7504 du CNRS-Université de Strasbourg,23 rue du Lœss, BP 43, 67034 Strasbourg Cedex 02, France*
[c]*The University of Da-Nang, University of Science and Technology, 54, Nguyen Luong Bang, Da-Nang, Viet Nam*
[d]*Unité de Catalyse et Chimie du Solide (UCCS), UMR 8181 du CNRS-Université de Lille-1, Bâtiment C3, Université Lille 1, 59655 - Villeneuve d'Ascq Cedex, France*
Corresponding author: cuong.pham-huu@unistra.fr (C. Pham-Huu)

Received (in XXX, XXX) Xth XXXXXXXXX 20XX, Accepted Xth XXXXXXXXX 20XX
DOI: 10.1039/b000000x

We report a high yield exfoliation of few-layer-graphene (FLG) with up to 17% from expanded graphite, under 5h sonication time in water, using graphene oxide (GO) as a surfactant. Aqueous dispersion of GO attached FLG (FLG-GO), with less than 5 layers, is used as a template for further decoration of nanodiamonds (NDs). The hybrid materials were self-organized into 3D-laminated nanostructures, where spherical NDs with diameter of 4-8 nm are homogeneously distributed on the surface of FLG-GO complex (referred to as FLG-GO@NDs). It was found that GO plays a dual role, it: (1) mediated exfoliation of expanded graphite in aqueous solution resulting in a FLG-GO colloid system, and (2) incorporated ND particles for the formation of composites. The high catalytic performance in the dehydrogenation of ethyl-benzene on FLG-GO@NDs metal-free catalyst is achieved; a 35.1% of ethylbenzene conversion and 98.6% styrene selectivity after 50 h reaction test is observed which corresponds to an activity of 896 $mmol_{ST}/g_{catalyst}/h$. It is 1.7 and 5 times higher than the unsupported NDs and traditional catalysts, respectively. The results demonstrate the potential of FLG-GO@NDs composite as a promising catalyst for steam- free industrial dehydrogenation applications.

Introduction

Graphene and few-layer graphene (FLG), containing different number of graphene layers up to thirty, have attracted a tremendous scientific interest due to their exceptional physical and chemical properties which allow them to be applied in several potential applications[1-3]. These materials can be synthesized by several methods, such as micromechanical cleavage[4], epitaxial growth on silicon carbide or metal surfaces[5-7], exfoliation of oxidized graphite and/or graphene oxide (GO)[8-11], mechanical ablation[12], and unzipping of mutliwalled carbon nanotubes[13-16]. Despite this large number of efforts, a mass production of graphene and FLG with low number of graphene layers by a versatile and low-cost method is still an active field of research, especially solution-phase method where graphene or FLG are directly obtained from exfoliation of graphite precursors [17,18]. This method, however, still has some drawbacks: (1) the synthesis is mostly carried out in organic solvents (e.g, MNP, DMF) which needs to be carefully recycled[19,20], (2) the low exfoliation yield (1-3 wt.%) despite a very long sonication time (few tens to hundred hours)[21,22], and (3) in the case of exfoliation of graphite in aqueous solution, the use of an amphiphilic surfactant which may affect the quality and needs further steps of treatments[23-25]. In fact, a direct exfoliation of hydrophobic graphite to graphene sheets in aqueous solution without dispersing agents has been considered to be extremely difficult or even unfeasible[26]. The ideas based on the use of GO as a dispersion agent for a stabilization of carbon materials, such as CNTs and graphite, has been recently done in few works. For example, Kim and co-workers reported for the first time that GO, with its amphiphilic nature, can act as a surfactant to process insoluble materials of graphite in aqueous solution[27,28]. It has been also reported that GO can act as a surfactant to prevent the aggregation of CNTs during the process[29]. Gogotsi and co-workers have performed an extensive reduction of GO attached on the expanded graphite (EG) surface through microwaves

irradiation[30]. However, the use of GO as physical agents for the synthesis of large scale single-to-few layer graphene, with a stable dispersion in a greener solvent, i.e. water, still represents a challenge to be tackled.

Synthetic NDs produced by detonation methods have an average size ranging of 4-10 nm, and their large surface-to-volume ratio endows them with higher surface reactivity than other form of carbon. Together with a large surface area, NDs also have high entropy, high structural defects content and low toxicity that make them a promising candidate for several applications in tribology, drug delivery, bio-imaging and tissue engineering just to cite the few of them[31]. Hybrid materials consisting of graphene and nanodiamonds (NDs) could potentially display not only the unique properties of NDs and those of graphene, but also additional novel properties due to the synergistic effects between them. Those materials are very interesting for future applications such as supercapacitors[32], photocatalysts[33,34], and electrocatalyst[35]. Recently, NDs have been reported by Su and co-workers[36] to be an efficient metal-free catalyst in the steam-free dehydrogenation of ethyl-benzene into styrene. The dehydrogenation mechanism can be described as follows: activation of the alkane fragment of the ethylbenzene by the ketone group to generate styrene along with the formation of carbon hydroxyl group as an intermediate followed by a release of hydrogen and the consecutive generation of the former C=O group. However, the NDs are used in powders form, aggregate forming clumps which could cause a considerable decrease of the active surface during the catalytic reaction. Thus the idea is to take advantage of the flat surface of graphene-based materials to disperse the ND particles, which would increase the effective contact surface and number of active sites, leading to enhancing their catalyst properties. Wang et al.[37] have reported that NDs are steadily dispersed onto reduced graphene oxide surface which leads to a significant improvement of the specific capacitance of the composite owing to the high exposed surface area and short diffusion length of the NDs.

In this work, we have tried to address three main aspects including: (1) a direct exfoliation of expanded graphite in aqueous solutions (with high yield and short sonication time) using GO as surfactants; (2) the use of GO attached few-layer-graphene (FLG-GO) aqueous dispersion as a template for further self-organized decoration of homogeneous nanodiamonds (NDs), and (3) such ND-decorated GO-FLG composites (referred to as FLG-GO@NDs) will be used as a metal-free catalysts in the steam-free dehydrogenation (DH) of ethylbenzene (EB) to styrene reaction which is one of the largest catalytic processes nowadays. Herein, GO acts as an adsorbent layer that concentrates ND nanoparticles on the surface of FLG-GO, meanwhile FLG plays a role of reinforcement support for GO which is easily shrinkage during NDs adsorption. The resulting 3D-sandwich structure of FLG-GO@NDs composite is tested as advancing catalyst in the DH of EB to styrene reaction. The activities are compared with the ones obtained from traditional catalysts. According to the results the FLG-GO@NDs composite displays predominant performances along with a high stability as a function of time on stream compared to the other catalysts. The present high-performance FLG-GO@NDs composite with great advantages such as simple and mass production method, and absence of cytotoxicity could be foreseen as a potential metal-free catalyst in the steam free industrial synthesis of styrene.

Experimental

Exfoliation of expanded graphite in aqueous medium using graphene oxide as a surfactant

Graphene oxide was prepared by a modified Hummer's method from flake graphite as described in supporting information (SI). A FLG-GO complex was prepared by aqueous solution-processed exfoliation of expanded graphite in GO suspension under ultrasonic treatment (see SI). Briefly, GO suspension with a concentration of 1 mg/mL was obtained by dispersing GO powders in distilled water with the aid of ultrasonic bath for 30 min. Then the different weight ratios of EG/GO, i.e. 1, 3, 5, were subjected to sonication with a tip sonicator of 30 W for different time ranging from 1 to 5 h. Subsequently, the as-prepared suspension was left to stand for 2 days to settling down unstable graphite aggregates. The supernatant was next extracted by pipette, and then centrifuged at 3000 rpm for 30 min to get the stable FLG-GO suspension which will be further processed.

Self-organized decoration of nanodiamonds on the FLG-GO sheets

The commercial nanodiamonds (NDs) with diameter in the range of 4-10 nm in a powder form were supplied by the Hightech Co (Finland) and were used without any further purification. For preparation of FLG-GO@NDs composite, typically 200 mg of pristine NDs were dispersed in 300 mL of deionized (DI) water followed by a sonication treatment for 30 min. It was then well mixed with a 286 mL as-synthesized FLG-GO complex suspension (0.35 mg/mL) by droplet under stirring condition. ND particles were steadily adsorbed in a homogeneous manner on the surface of FLG-GO and the resulted composite settled down after few minutes. The adsorption of the NDs on the GO-FLG surface was evidenced by the change of the solution color from yellow-pale (NDs solution) to colorless. The mixture was then filtered and dried at 100 °C in the oven for 6 h to get a constant weight of the FLG-GO@NDs composite.

Characterization techniques

UV-vis spectra were recorded using a spectrophotometer equipped with Peltier PTP1 system (PerkinElmer Lambda 35) at room temperature. X-ray diffraction (XRD) data were collected on a Bruker D8 Advance diffractometer. X-ray photoelectron spectroscopy (XPS) measurements were performed with ESCA2000 (VG Microtech) spectrometer using a monochromatized aluminum Kα anode. Thermal gravimetric analysis (TGA) was carried out on a TGA Q5000 instrument with a heating rate of 10 °C min^{-1} under air atmosphere. The specific surface area was measured using the BET method from nitrogen adsorption-desorption isotherm at 77K (TriStar sorptometer). Prior to measurement, the sample was out-gassed at 250 ^{o}C during 12 hours in order to desorbed moisture and/or other impurities. The Raman spectra were recorded using LabRAM ARAMIS Horiba Raman spectrometer equipment. Spectra were recorded over the range of 500 - 4000 cm^{-1} at the laser excitation wavelength of 532 nm. The sample was deposited on glass substrate by spin-coating of its suspension and carefully dried

before measurement. Scanning electron microscopy (SEM) images were recorded using a JEOL 2600F instrument operating at an acceleration voltage of 15 kV and an emission current of 10 mA. The sample was covered with a thin layer of sputtered gold in order to avoid charging problems during the analysis. Transmission electron microscope (TEM) was conducted on JEOL 2100F working at 200 kV accelerated voltage, equipped with a probe corrector for spherical aberrations, and a point-to-point resolution of 0.2 nm. The sample was dispersed in ethanol with the aid of mild sonication for 5 minutes and a drop of the suspension was deposited on a holey carbon grid for measurement.

Catalytic activity measurements

The steam-free catalytic dehydrogenation of ethyl-benzene to styrene was carried out in a tubular quartz reactor (74 cm length and 1.2 cm I.D.) under atmospheric pressure at 550°C. The catalysts (300 mg) were deposited on a quartz wool plug and the reactant passed downward through the catalyst bed. Before reaction, the catalyst was slowly heated up to the reaction temperature and pretreated at 550°C under helium for 2 h. The reactant flow (2.8 vol. % EB diluted in helium, with a total flow rate of 30 mL. min^{-1}) was then fed to the reactor. The reactants and the products, exit from the reactor, was analyzed on–line with a PERICHROM (PR 2100) gas chromatography equipped with a flame ionization detector (FID). In order to avoid any possible condensation of the reactant or products, all the tube lines were wrapped with a heating wire kept at 110°C.

The ethyl-benzene conversion (X_{EB}), styrene selectivity (S_{ST}) and yield (Y_{ST}) were evaluated using the following equations:

$$X_{\mathrm{EB}} = \frac{F_0 C_{EB,inlet} - F C_{EB,outlet}}{F_0 C_{EB,inlet}} \times 100\% \quad (1)$$

$$S_{\mathrm{ST}} = \frac{C_{ST,outlet}}{C_{ST,outlet} + C_{TOL,outlet} + C_{BZ,outlet}} \times 100\% \quad (2)$$

$$Y_{ST} = X_{EB} \times S_{ST} \quad (3)$$

where F and F_0 are the inlet and outlet flow rates; C_{EB}, C_{ST}, C_{TOL} and C_{BZ} represents the concentration of ethyl benzene, styrene, toluene and benzene, respectively. The specific rate is expressed as amount of styrene produced per gram of catalyst per hour ($mmol.g^{-1}.h^{-1}$).

Results and Discussion

The FLG was synthesized by mild sonication at 40 °C of aqueous mixtures containing EG and GO with different weight ratios, i.e. 1:1, 3:1 and 5:1 (supporting information, SI). The sonication was kept for different durations and the products issued from these treatments were collected for subsequence analysis. Figure 1A shows the digital photo of the EG/GO mixtures after 5 h of sonication, it highlights the extremely high dispersion of the resulted materials when GO was added to the EG suspension: indeed no precipitation was observed after several weeks of standing. On the other hand, the FLG formed from the EG suspension in water, without adding GO, and after the same sonication treatment, steadily precipitates after a few tens of minutes due to its hydrophobic nature and strong attraction forces. Similar results have also been observed by Hu et al.[30] during the sonication process with a EG:GO mixtures with a high GO concentration. The high stability of the obtained FLG could be explained by a number of physical methods that clearly demonstrated the production of single-to-few-layer graphene as shown in the schematic exfoliation process (schematic 1, SI).

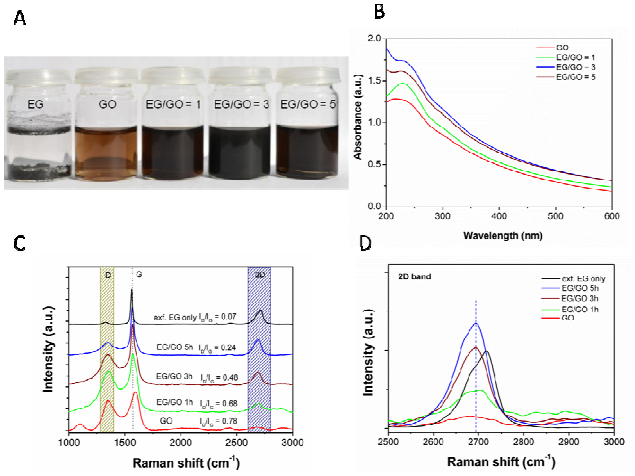

Figure 1. (A) A digital photo of the different EG/GO mixtures in aqueous medium after sonication for 3h. (B) UV-vis spectra of the different EG/GO mixtures which show the degree of the EG exfoliation, (C and D) Raman spectra recorded on different samples according to sonication time and the enlargement of the 2D peak.

The formation of stable FLG-GO suspension as a function of EG/GO was monitored by UV-vis spectroscopy as depicted in Figure 1B. The broad π-π* transition of aromatic C=C peak of GO centered at 230 nm^{-1} is gradually red shifted several nm up to 238 nm when the EG/GO ratios increase from 0 to 5. The absorption intensity increased as well, and the highest intensity is observed with a mixture of EG/GO equal to 3; that shows the best dispersion degree of EG/GO and the stabilization of exfoliated FLG in the solution. When the EG/GO ratio is higher or lower than 3 (i.e., 5, 1), the absorption intensity tends to get down, suggesting lower concentration of chromophores in the suspension, so a lower stabilization of the FLG sheets. The degree of exfoliation as a function of sonication time was also investigated for the EG/GO ratio equal 3 as shown in Figure S1A (SI). The amount of FLG in the FLG-GO complex increased up to 0.35 mg/mL for 5h sonication, and then exhibited plateau trend for longer sonication time (Figure S1B). The optical absorbance (A) divided by the length (l) as a function of the concentration for aqueous suspension FLG-GO shows a Lambert-Beer behavior, and a linear fit of the concentration values gives an average absorption coefficient at 660 nm of α = 2,244 $Lg^{-1}m^{-1}$ (Figure S1C), which is consistent with the value measured for previous exfoliation of graphene in NMP[19].

The XRD patterns of the as-synthesized materials as a function of the EG:GO ratio are presented in Figure S2. The patterns showed that a 2θ peak of GO at 11° was gradually decreased when the EG/GO ratio increased, while two peaks corresponding to (002) and (004) reflection of graphite are increased consecutively. It means that the crystallinity of the FLG-GO

complex increased as a function of EG/GO ratio, and when the ratio EG/GO reached 5, it would correspond to a large graphite-like structure in the products, which is consistent with the UV-vis measurements. The layer thickness and structural change of FLG-GO films as a function of sonication time, compared to its precursor materials (exfoliated EG and GO), were efficiently monitored by Raman spectroscopy (Figure 1C). While the Raman spectrum shows a typical D-band at 1345 cm^{-1} (sp^3 defects) and G-band at 1592 cm^{-1} (tangential vibration of sp^2 carbon atoms) for GO, those peaks are appeared at 1350 and 1580 cm^{-1} respectively for FLG. A comparison of the intensity ratio of D and G band (I_D/I_G) as a function of sonication time for all samples was also performed. The I_D/I_G decreased from 0.78 for pure GO to 0.24 for FLG-GO complex after 5 h sonicating confirming the better graphitic behavior of the sample. In addition, the G-band of FLG-GO complex was red shifted (8 cm^{-1}) and blue shifted (12 cm^{-1}) as compared to that of FLG and GO, respectively, which confirms a physical interaction of GO and the FLG sheets. The π-conjugated aromatic domains existing in GO basal plane interacts with the surface of FLG via π–π interactions[28,30]. Moreover, it is known that the 2D band corresponds to the specific numbers of stacked graphene films[38]. As compared to exfoliated EG, the 2D peak positions in FLG-GO shifted considerably to a lower wavenumber by 25 cm^{-1}, from 2718 to 2693 cm^{-1}, and the intensities of symmetric peaks are higher than with FLG after 3h sonication, suggesting a successful exfoliation to less than 5 layers FLG in FLG-GO complex[18,39]. All above results have shown that GO sheets significantly promotes the effective exfoliation of EG in aqueous solution after relatively short time of sonication. The excellent water solubility of GO made the FLG-GO complex to have a micelle system-like behavior.

Representative TEM micrographs of the as-synthesized FLG decorated with GO sheets are presented in Figure 2. They confirm the high degree of exfoliation of the process as almost FLG containing less than five graphene layers is observed among the sample (Figure 2A). High-resolution TEM micrographs also evidence the non-covalent stacking between the FLG and GO as presented in Figure 2B and 2C, where a perfect graphitized structure of the FLG is visible underneath the disordered structure of the GO. The nature and concentration of the oxygen species present on the different samples were also analyzed by XPS and the results are presented in Figure 2D and E. The C1s XPS spectrum of the GO, with oxygen content ~32.6 at. %, is presented in Figure 2D and can be deconvoluted into four peaks corresponding to carbon atoms in different functional groups: the C-C in aromatic rings, the oxygenated C in C-O, C=O, and O-C=O. However, the high percentage of oxygen in the GO was steadily decreased in the FLG-GO complex (Figure 2E), with an oxygen content of ~ 8.3 at. %. In addition, the ratio of C/O obtained from the C1s and O1s peaks increased from 2 (for GO) to 10 (for FLG-GO), respectively. Such a result could be attributed to the intimate mixing between the GO and the exfoliated FLG with low oxygen content. It is expected that during the sonication process, a part of the oxygen content could also be removed from the GO surface due to the energy input.

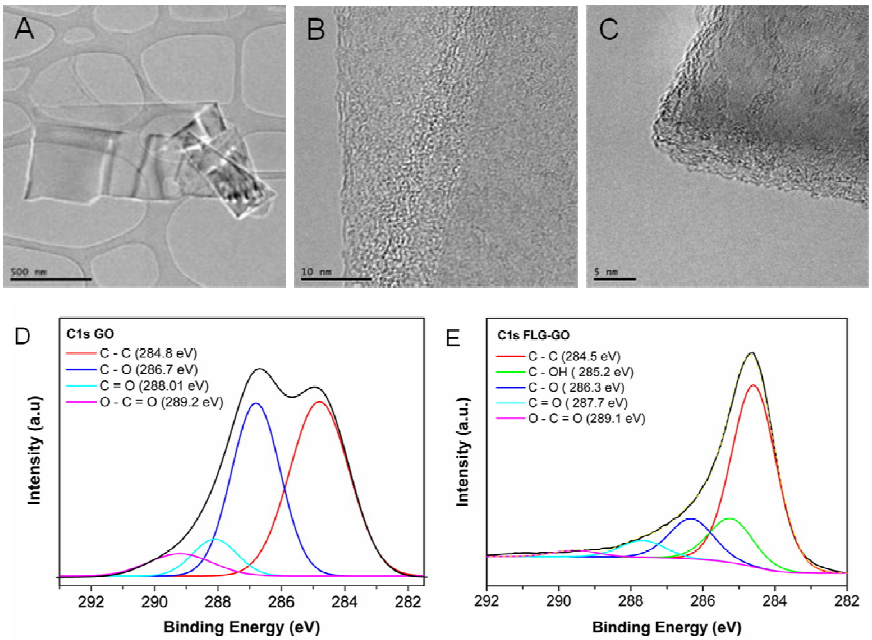

Figure 2. (A-C) Representative TEM micrographs of the GO mediated exfoliated EG with different magnifications. (D and E) C1s XPS spectra of the GO and FLG-GO showing a strong reduction of the oxygen functional groups along with the increase of the carbon species after mixing.

The yield of the exfoliation process as a function of the sonication duration is presented in Figure 3. The FLG exfoliation yield was calculated based on the weight of initial and final materials as defined in Eq. 4:

$$exf(\%) = \frac{ini(EG+GO) - (unexfEG + setl.exfMLG@GO)}{ini(EG+GO)} 100\% \quad (4)$$

Where *ini*(EG+GO) is the initial mass sum of EG and GO before sonication, *unexf*EG is the un-exfoliated EG decanting after 2

days standing, and *setl.exf*MLG@GO is the GO absorbed on multi-layer-graphene that settled down after centrifugation at 3000 rpm. The exfoliation of EG that was calculated according to equation (4) increase from 2.2, 5.3, 8.8, 12.3 to 16.8 wt% relative to the initial raw materials (EG added GO) for sonication time ranging from 1, 2, 3, 4 to 5 hours, respectively. The exfoliation yield was also measured by UV-vis on the different concentration of FLG-GO suspensions (Figure 3B). The red line is a linear fit in which the yield is relative to initial EG (if assumed that no GO was decanted during the synthesis process), while the blue line is the yield relative to the total EG-GO mass. The exfoliation yield increases with sonication time, and that reaches the value of up to ~ 25 wt% of the relative to the initial EG after 5h sonication. The GO mass percentage in FLG-GO mixture can be estimated at 25 wt % after 5 h sonication. This data is consistent with TGA measurement as shown in Figure S3, in which the curve corresponding to the GO has onset temperature at 130 and 450 ^{o}C, which can be related to the decomposition of different oxygen containing groups, while the onset temperatures of GO-FLG complex are increased and appeared at 360 and 560 ^{o}C. The amount of GO in the GO-FLG complex is estimated to be about 24 % by mass. According to the results one can states that GO mediated EG exfoliation process is among the best method to obtain thin FLG with high yield and under mild treatment time.

From the reported results, we have shown that a thin FLG-GO complex was successfully prepared in aqueous suspension medium by the solution-phase method. The as-synthesized FLG-GO mixture is used as a template for further self-organized decoration FLG-GO with homogeneous nanodiamonds (NDs), for applying as a metal-free catalyst in the steam-free dehydrogenation (DH) of ethyl benzene (EB) to styrene reaction.

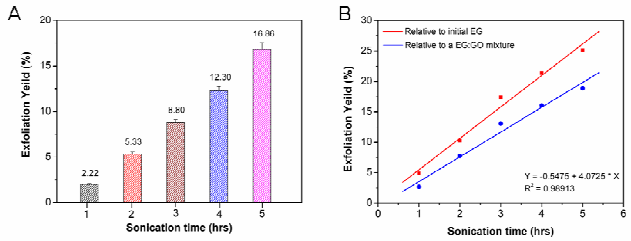

Figure 3. Exfoliation yield of EG calculated with the Eq.4 (A), data calculated from the maximum concentration relative to starting materials and fit linear (B).

Figure 4A shows a digital photo of aqueous dispersion of pristine NDs after 15 min tip sonication (Fig. 4A, left), and a colloidal suspension of FLG-GO (3-1) complex (Fig. 4B, middle). When the NDs dispersion (2 parts) is dropped into FLG-GO suspension (1 part) under stirring conditions, ND particles are steadily adsorbed onto the surface of FLG-GO complex, which results in the precipitation of the FLG-GO@NDs (1:2) product in water (Fig. 4C, right). The complete adsorption of the NDs was evidenced by the colour change from yellow-pale to colourless of the medium upon precipitation. Herein, the aqueous dispersion of NDs has a positive charge with a zeta potential of +16 mV, whereas FLG-GO suspension is negatively charged (–46 mV); thus, the interaction between them can be considered as electrostatic attractions (a zeta potential of re-dispersed FLG-GO@NDs suspension shows a value of -28 mV (Figure S4A)).

Other possible interactions between FLG-GO and NDs may be hydrogen-bond attractions because of the presence of oxygen-containing groups including hydroxyl, carboxylic, lactones, ketones and ethers[31,40] on the surface of NDs which can be strongly interacted with the GO surface.

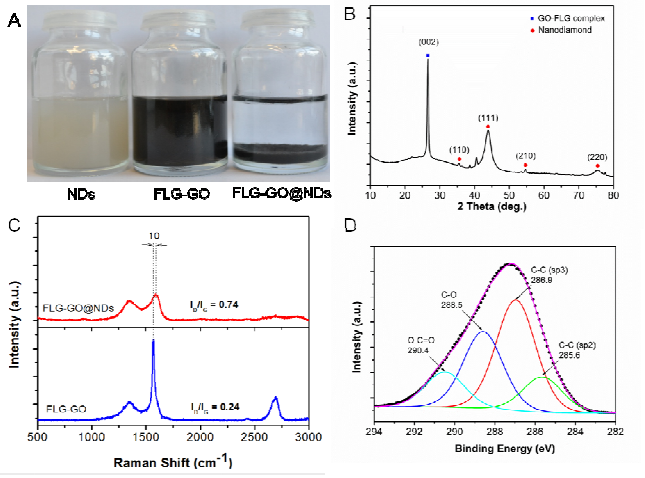

Figure 4. (A) A digital photo of aqueous dispersion of pristine NDs (left), FLG-GO complex suspension (middle) and ND-absorbed FLG-GO (right). (B) XRD spectra, (C) Raman spectrum and (D) C1s XPS spectrum of FLG-GO@NDs composite.

It should be noted that NDs are not adsorbed on the surface of FLG under similar conditions (Figure S4B). The microstructure of FLG-GO@NDs composite was investigated by SEM (Figure S5), which shows that the FLG-GO powders consist of thin FLG platelets covered by a slightly wrinkled GO layer. The FLG-GO@NDs showed 3D laminated structures where the GO sheets were homogeneously decorated with ND particles. The XRD pattern of FLG-GO@NDs is shown in Figure 4B, while the strong diffraction peak at $2\theta = 26.5°$ is attributed to the (002) reflection from the graphite, the other peaks correspond to NDs self-organized adsorption on the surface of FLG-GO support. Raman spectroscopy at λ_{exc} = 532 nm was employed to investigate a change in the graphitic structure after adsorption of NDs, as shown in Figure 4C. The Raman spectrum of FLG-GO@NDs shows an increased intensity and a broadening of sp^3 defects (D-band) as compared with FLG-GO complex since it overlapped with a peak of ND itself (~1324 cm^{-1}). The tangential vibration of sp^2 carbon atoms in hexagonal plane (G-band) is noteworthy decreased, and the I_D/I_G ratio increases more than 3 times from 0.24 to 0.74. It reflects that NDs cover the surface of FLG-GO and that the vibration of the graphitic domains is considerably attenuated. In addition, G-band shifted of about 10 cm^{-1} to a higher wavenumber, the reason may come from the functional groups on the surface of NDs such as O-H bending and C=O stretching[31]. The composition of FLG-GO@NDs composite was analyzed by XPS and the results are presented in Figure 4D. The C1s XPS spectrum clearly indicates four different major components (C sp^2, C sp^3, C-O and O=C-O), in which the non-oxygenated sp^2 carbon of graphene is noteworthy decreased when compare to the FLG-GO complex, whereas the sp^3 allotrope of carbon at 286.9 eV becomes a prominent peak. This peak corresponds to the NDs incorporation.

The dispersion of the NDs on the surface of the FLG-GO has

been characterized by TEM microscopy (Figure 5). It is clearly seen that the FLG-GO sheets are homogeneously decorated by spherical ND particles. Herein, the GO acts as an adsorption layer for randomly distributed NDs on the surface of FLG-GO complex, while FLG plays the role of inactive support to strengthen the FLG-GO complex, i.e. to hinder the GO layers shrinkage during NDs adsorption. The high anchorage strength of the NDs onto the GO surface could be attributed to the presence of OH groups on the NDs surface. Wang et al.[37] have reported that those OH groups also actively participate in the reduction process of the GO after further heating treatments.

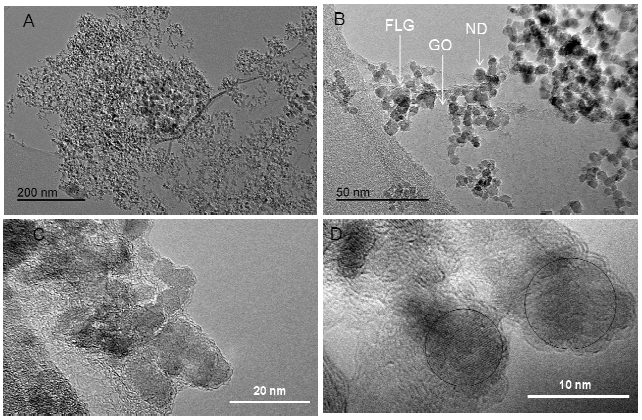

Figure 5. Representative TEM micrographs of the FLG-GO@NDs composite with different magnifications. (A) General view showing the homogeneous dispersion of the NDs on the composite surface. (B) Medium view evidencing the high affinity of the NDs to adsorb on the GO surface. (C-D) High-resolution views showing the microstructure of the NDs and a detail view of the NDs' top surface

From higher magnification TEM images, it can be seen that the ND nano-crystallites with average diameter ranging from 4 to 8 nm are isolated over FLG-GO sheets. A distribution of ND particles size has been measured using *Image-Pro Plus* program on TEM images and presented in Figure S6. This is an important factor for a significant improvement of catalyst performances of the FLG-GO@NDs which will be considered in the following.

In order to evaluate catalytic performance of the FLG-GO supported NDs catalyst in the dehydrogenation of ethyl-benzene, 300 mg of the composite material were placed at the centre of a quartz reactor. The reaction was carried out at 550 ^{o}C under atmospheric pressure, conditions similar as those reported by Su et al.[36]. The reaction rate was expressed as the amount of styrene produced per gram of catalyst per hour. The catalyst selectivity to styrene has been also investigated. Figure 6A shows a comparison of the styrene formation rate (ST. rate) and styrene selectivity (ST. Sel.) on the FLG-GO@NDs composite-based catalyst versus those obtained on unsupported NDs and commercial iron-based catalysts (denoted as K-Fe). It was observed that the K-Fe catalyst exhibits extremely high DH activity at the beginning of the test (853 $mmol_{ST}/g_{catalyst}/h$) followed by a sharp deactivation to be next stabilized after 8 h of reaction at around 180 $mmol_{ST}/g_{catalyst}/h$. The low DH activity obtained on the iron-based catalyst could be attributed to the rapid saturation of the active sites by carbonaceous residue under steam-free reaction conditions. On the other hand, both the unsupported NDs and FLG-GO@NDs composite-based catalysts display a significant improvement of the DH activity, compared to the K-Fe catalyst, with a gradually decrease from 1064 to 402 $mmol_{ST}/g_{catalyst}/h$ and 1680 to 687 $mmol_{ST}/g_{catalyst}/h$, respectively, after the same duration of test, i.e. 50 h of time on stream. However, in contrary to the commercial catalyst, ND-based catalysts display a slow deactivation after the first deactivation slope. Such observation indicates that site blockage as a function of time on stream still occurs unlikely to the industrial catalyst where a balance of site blockage by deposited carbonaceous residue was reached after few hours of reaction. The significant improvement of the DH activity per unit weight of the NDs obtained on the supported FLG-GO catalyst could be attributed to the higher dispersion of the NDs on the GO surface, as evidenced by SEM and TEM analysis presented above. The dehydrogenation rate as a function of time on stream observed on both catalysts, NDs and FLG-GO@NDs, is similar which indicates that the nature of the active site is unchanged and the DH activity improvement is mostly due to the higher active sites on the FLG-GO@NDs consecutive to the dispersion of the NDs on the FLG-GO surface. This provides higher specific surface area and density of active sites to perform the dehydrogenation reaction. The BET value increased from 283 m^2/g for pristine NDs to 304 m^2/g for FLG-GO@NDs along with a significant rise in mesoporous contribution (Figure S7). In the FLG-GO@NDs catalyst the FLG with higher mechanical strength play a role of inactive support to prevent the clumping of the catalyst. To confirm our discussion on the role of FLG in the composite, a GO@NDs (without FLG) sample was tested under same reaction condition (Figure S8). The GO@NDs catalyst exhibits an intermediate DH activity compared to the NDs and FLG-GO@NDs catalysts. The low DH activity on the GO@NDs catalyst might be linked to the fact that GO clumped during adsorption of NDs, without FLG underneath, which will be limited the density of active sites and thus, leading to the lower DH performance.

The steady-state DH activity of the FLG-GO@NDs catalyst was compared also with those obtained on different carbon-based and K-Fe catalysts (Figure 6B). The results evidence the high DH activity of the FLG-GO@NDs catalyst compared to the other carbon-based nanomaterial catalysts such as stacked GO, thick FLG, and CNTs. The high DH activity observed on the ND-based catalyst could be attributed to the high effective surface area of the catalyst and also to the high stability of the oxygenated functional groups on the NDs surface compared to that existed on the other carbon-based materials.

The stability of FLG-GO@NDs catalyst as a function of time on stream is also evaluated by performing long-term test up to 150 h (Figure 6C). The DH activity was stabilized at around 500 $mmol_{ST}/g_{catalyst}/h$, after 150 h of test, while the selectivity towards styrene remains unchanged for the whole test. Such results indicate that the deactivation was mostly linked with the lost of active sites and not to a modification of the active site nature.

The DH activity can be recovered by submitting the spent catalyst to regeneration process in air at 400 °C for 2 h (Figure 6D). It is also worthy to note that successive regenerations contribute also to a better stability of the catalyst as a function of time on stream, as evidenced in Figure 6D. Similar behavior has been also reported by Su and co-workers[36] in a previous report.

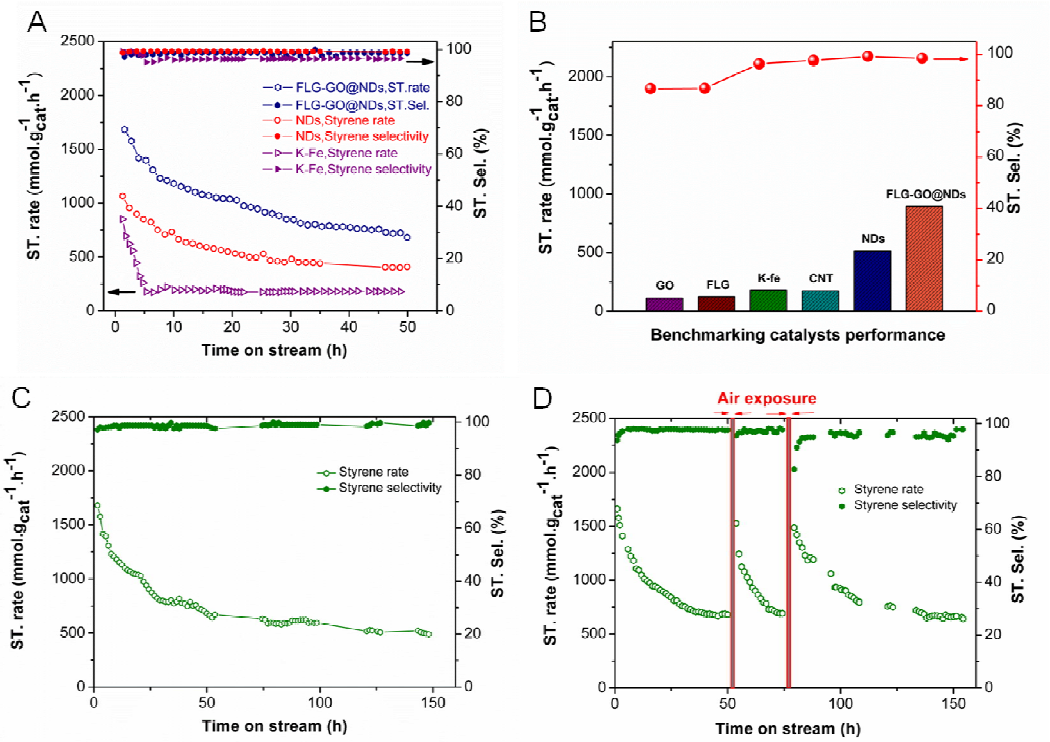

Figure 6. (A) DH activity of FLG-GO@NDs in comparison with commercial, unsupported NDs catalysts, (B) Benchmarking of different carbon-based nanomaterials in the DH process, (C) Long-term DH test at 550 °C of the FLG-GO@NDs catalyst, and (D) Regeneration test during cyclic air-exposure showing a high DH activity recovery of the GO-FLG@NDs-based composite catalyst.

In order to understand the cause of the deactivation and the regeneration mechanism, the XPS analysis was performed on the catalyst at different stage, i.e. fresh, spent and regenerated catalyst, and the results are shown in Figure S9. As can be seen from the XPS data, the carbon-to-oxygen ratio on the catalyst steadily increases from 13.8 for the fresh catalyst to18.6 for the one after reaction. Such results indicate that carbonaceous species were deposited onto the catalyst surface during the course of the reaction which slowly covers the surface of the active sites leading to catalyst deactivation. It is also worthy to note that during the reaction part of the oxygen species presents on the catalyst surface, especially the quinoic group which is expected to be the active site, could be also removed. The C/O ratio steadily decreases from 18.6 to 7.7 after regeneration process indicating that part of the carbonaceous residues has been removed, leading to a higher active site exposure. The change in the oxygen-containing functional groups, such as C-O and O-C=O, is well matched with the DH activity behaviour observed on the catalyst performances. According to the results, the decrease of the oxygenated functional groups, especially carboxylate group, is well fitted with the decrease of the DH activity of the catalyst. The C=O groups slightly decrease from 11 to 8 at. % which corresponds to the decrease of the DH activity from 1680 $mmol_{ST}/g_{catalyst}/h$ to 687 $mmol_{ST}/g_{catalyst}/h$. After regeneration, the C=O functional groups steadily increase from 8 to about 57 at. % while the DH activity is fully restored (Figure 6D). Our results are consistent with those previously reported by Su and co-workers in which the reduced DH activity agrees well with the consumption of C=O content[36]. The physical properties of the spent catalysts have been evaluated by XPS and temperature-programmed oxidation (TPO) techniques. The XPS results of the oxygen-based species recorded from the different samples, as-received FLG-GO@NDs, pre-treated at 550 °C under He and post-reaction FLG-GO@NDs composite are summarized in Figure S10. It showed that the O-H bond of the FLG-GO@NDs was remained unchanged, for the sample before and after reaction, at about 7.9 at. %, which indicates that hydrogenation of the catalyst, during the course of the reaction, was unlikely to occur. In addition, the TPO mass spectrum of the post-reaction composite displayed no peak H_2O during the combustion, which suggested that hydrogen generated from the reaction was directly released out from the catalyst.

Conclusion

We have demonstrated in this report an easy and scalable method to produce a “sandwich structured” between GO and FLG, where GO plays the role of dispersant allowing the exfoliation of expanded graphite into thin FLG structure and prevents the re-stacking of the FLG. The GO layer also provides anchorage sites for adsorbing ND particles through a charge compensation leading to the high dispersion of this later on the hybrid support surface. The NDs/GO/FLG composite was further used as a metal-free catalyst in the steam-free dehydrogenation of ethyl- benzene to styrene. The hybrid composite exhibits a high and relatively stable DH performance compared

to the other carbon-based and doped iron industrial catalysts. The DH activity per weight unit of NDs was about two times higher than the one obtained on the unsupported, which is due to the high dispersion of the NDs on the GO-FLG surface. The NDs/GO/FLG also exhibits a relatively high DH stability as a function of time on stream, up to 150 h. The deactivated catalyst can be efficiently regenerated by air calcinations at 400 °C which allows the recovery of the C=O functional groups and the removal of the carbonaceous residues deposited during the course of the reaction. The results obtained in the present work can be further extended to other liquid-phase catalytic applications where high reactive surface of the GO is required for adsorption of metal nanoparticles.

Acknowledgements

Tung T. T and Lai T. P. would like to thank the European Union for the grant through the Freecats project (NMP-2011-22.4). The SEM and TEM analysis were performed at the facilities of the IPCMS (UMR 7504 CNRS-University of Strasbourg) and T. Romero (ICPEES) is gratefully acknowledged for performing SEM analysis; P. Bernhardt (ICPEES) is gratefully acknowledged for performing XPS analysis.

References

1. K. S. Novoselov, A. K. Geim, S. V. Morozov, D. Jiang, M. I. Katsnelson, I. V. Grigorieva, S.V. Dubonos and A.A. Firsov. Two-dimensional gas of massless Dirac fermions in graphene. Nature 2005, 438**,** 197–200.
2. A. K. Geim and K. S. Novoselov. The rise of graphene. Nat. Mater. 2007, 6, 183-91.
3. F. Schedin, A. K. Geim, S. V. Morozov, E. W. Hill, P. Blake, M. I. Katsnelson and K. S. Novoselov. Detection of individual gas molecules adsorbed on graphene. Nat. Mater. 2007, 6, 652-655.
4. K. S. Novoselov, A. K. Geim, S. V. Morozov, D. Jiang, Y. Zhang, S. V. Dubonos, et al. Electric field effect in atomically thin carbon films. Science 2004, 306, 666-669.
5. C. Berger, Z. M. Song, X. B. Li, X. S. Wu, N. Brown, C. Naud, et al. Electronic confinement and coherence in patterned epitaxial graphene. Science 2006, 312, 1191–1198.
6. B. Dlubak, M. Martin, C. Deranlot, B. Servet, S. Xavier and R. Mattana. Highly efficient spin transport in epitaxial graphene on SiC. Nature Physics 2012, 8, 557-561
7. N. C. Bartelt and K. F. McCarty. Graphene growth on metal surfaces. MRS Bulletin 2012, 37, 1158-1165
8. Park, S.; Ruoff, R. S. Chemical methods for the production of graphenes. Nature Nanotech. 2009, l4, 217-224
9. W. Gao, L. B. Alemary, L. Gi, P. M. Ajayan. New insights into the structure and reduction of graphite oxide. Nature chem. 2009, 1, 403-408
10. S. Stankovich, D. A. Dikin, R. D. Piner, K. A. Kohlhaas, A. Kleinhammes and Y. Jia. Synthesis of graphene-based nanosheets via chemical reduction of exfoliated graphite oxide. Carbon 2007, 45, 1558-1565
11. J. T. Robinson, F. K. Perkins, E. S. Snow, Z. Wei and P. E. Sheehan. Reduced graphene oxide molecular sensors. Nano lett. 2008, 8, 3137-3140
12. I. Janowska, F. Vigneron, D. Bégin, O. Ersen, P. Bernhardt, T. Romero, et al. Mechanical thinning to make few-layer graphene from pencil lead. Carbon 2012, 50, 3106-3110
13. D. M. Kosynkin, A. L. Higginbotham, A. Sinitskii, J. R. Lomeda, A. Dimiev, B. K. Price, et al. Longitudinal unzipping of carbon nanotubes to form graphene nanoribbons. Nature 2009, 458, 872–876.
14. L. Jiao, L. Zhang, X. Wang, G. Diankov and H. Dai. Narrow graphene nanoribbons from carbon nanotubes. Nature 2009, 458, 877–880
15. L. Jiao, X. Wang, G. Diankov, H. Wang and H. Dai. Facile synthesis of high-quality graphene nanoribbons. Nature Nanotech. 2010, 5, 321 – 325
16. I. Janowska, O. Ersen, T. Jacob, Ph. Vénnégues, D. Bégin, et al. Catalytic unzipping of carbon nanotubes to few-layer grapheme sheets under microwaves irradiation. Appl. Catal. A: Gen. 2009, 371, 22-30.
17. L. Jaber-Ansari, M. C. Hersam. Solution-processed graphene materials and composites. MRS Bulletin 2012, 37, 1167-1175.
18. C. Shih, A. Vijayaraghavan, R. Krishnan, R. Sharma, J. H. Han, M. H. Ham. Bi- and trilayer graphene solutions. Nature Nanotech. 2011, 6, 439-445.
19. Y. Hernandes, V. Nicolosi, M. Lotya, F. M. Blighe, Z. Sun, et al. High-yield production of graphene by liquid-phase exfoliation of graphite. Nature Nanotech. 2008, 3, 563-568.
20. J. N. Coleman. Liquid exfoliation of defect-free graphene. Acc Chem Res. 2013, 46, 14-22.
21. A. O'Neill, U. Khan, P. N. Nirmalraj, J. Boland, J. N. Coleman. Graphene dispersion and exfoliation in low boiling point solvents. J. Phys. Chem. C, 2011, 115, 5422–5428
22. U. Khan, A. O'Neill, M. Lotya, S. De, J. N. Coleman. High-concentration solvent exfoliation of graphene. Small 2010, 6, No. 7, 864-871
23. M. Lotya, P. J. King, U. Khan, S. De, J. N. Coleman. High-concentration, surfactant-stabilized graphene dispersions. ACS Nano 2010, 4, 3155-3162.
24. M. Lotya, Y. Hernandez, P. J. King, R. J. Smith, V. Nicolosi, L. S. Karlsson, et al. Liquid phase production of graphene by exfoliation of graphite in surfactant/water solution. J. Am. Chem. Soc. 2009, 131, 3611-3620
25. A. A. Green, M. C. Hersam. Solution phase production of graphene with controlled thickness via density differentiation. Nano Lett. 2009, 9, 4031-4036
26. D. Li, M. B. Muller, S. Gilje, R. B. Kaner, G. Wallace. Processable aqueous dispersions of graphene nanosheets. Nature Nanotech. 2008, 3, 101-103
27. J. Kim, L. J. Cote, F. Kim, W. Yuan, K. R. Shull, J. Huang. Graphene oxide sheets at interfaces. J. Am. Chem. Soc. 2010,132, 8180-8186
28. L. J. Cote, J. Kim, V. C. Tung, J. Luo, F. Kim, J. Huang. Graphene oxide as surfactant sheets. Pure Appl. Chem. 2011, 83,1, 95-110
29. S. H. Lee, D. H. Lee, W. J. Lee, S. O. Kim. Tailored assembly of carbon nanotubes and Graphene. Adv. Func. Mat. 2012, 21, 1338-1354
30. H. Hu, Z. Zhao, Q. Zhou, Y. Gogotsi, J. Qiu. The role of microwave absorption on the formation of graphene oxide. Carbon 2012, 50, 3267-3273
31. V. N. Mochalin, O. Shenderova, D. Ho and Y. Gogotsi. The properties and applications of nanodiamonds. Nature Nanotech. 2012, 7, 11-23
32. Y. Sun, Q. Wu, Y. Xu, H. Bai, C. Li, G. Shi. Highly conductive and flecxible mesoporous graphitic films prepared by graphitizing the composites of graphene oxide and nanodiamond. J. Mater. Chem. 2011, 21, 7154-7160.
33. D. M. Jang, J. Myung, H. S. Im, Y. S. Seo, Y. J. Cho, C. W. Lee, J. Park, A. Y. Jee and M. Lee. Nanodiamonds as photocatalysts for reduction of water and graphene oxide. Chem. Commun. 2012, 48, 696-698.
34. D. M. Jang, H. S. Im, J. Myung, Y. S. Seo, Y. J. Cho, H. S. Kim, S. H. Back, J. H. Park, E. H. Cha, M. Lee. Hydrogen and carbon monoxide generation from laser-induced graphitized nanodiamonds in water. Phys. Chem. Chem. Phys. 2013, 15, 7155-7160
35. J. Zang, Y. Wang, L. Bian, J. Zhang, F. Meng, Y. Zhao, R. Lu. X. Qu, S. Ren. Graphene growth on nanodiamonds as a support for a Pt electrocatalyst in methanol electro-oxidation. Carbon 2012, 50, 3032-3038.

36. J. Zhang, D. S. Su, R. Blume, R. Schlögl, R. Wang, X. Yang, A. Gajović. Surface chemistry and catalytic reactivity of a nanodiamond in the steam-free dehydrogenation of ethylbenzene. Angew. Chem. Int. Ed. 2010, 49, 8640-8644
37. Q. Wang, N. Plylahan, M. V. Shelke. R. R. Devarapalli, M. Li, et al. Nanodiamond particles/reduced graphene oxide composites as efficient supercapacitor electrodes. Carbon 2014, 68, 175-184.
38. A. C. Ferrari, D. M. Basko. Raman spectroscopy as a versatile tool for studying the properties of graphene. Nature Nanotech. 2013, 8, 235-243
39. A. C. Ferrari, J. C. Meyer, V. Scardaci, C. Casiraghi, M. Lazzeri, F. Mauri, S. Piscanec, D. Jiang, K. S. Novoselov, S. Roth, A. K. Geim. Raman spectrum of graphene and graphene layers. Phys. Rev. Lett. 2006, 97, 187401-1-4
40. Y. Liu, Z. Gu, J. L. Margrave, V. N. Khabashesku. Functionalization of nanoscale diamond powder: fluoro-, alkyl-, amino-, and amino acid-nanodiamond derivatives. Chem. Mater. 2004, 16, 3924–3930

.